



Article

Effect of Channel Shape on Heat Transfer and Mechanical Properties of Supercritical CO₂ Microchannel Heat Exchanger

Peiyue Li ¹, Wen Fu ¹, Kaidi Zhang ², Qiulong Li ¹, Yi Zhang ¹, Yanmo Li ¹, Zhihua Wang ¹, Xiuhua Hou ¹, Yuwei Sun ²  and Wei Wei ^{2,*} 

¹ Luoyang Ship Material Research Institute (LSMRI), Luoyang 471000, China; lpy110015@163.com (P.L.); angle_fw@163.com (W.F.); liquilongcsu@163.com (Q.L.); zhangyicsu@163.com (Y.Z.); warriormo@163.com (Y.L.); 16603790401@163.com (Z.W.); 15036736339@163.com (X.H.)

² State Key Laboratory of Maritime Technology and Safety, Wuhan University of Technology, Wuhan 430063, China; zkd@whut.edu.cn (K.Z.); ywsun@whut.edu.cn (Y.S.)

* Correspondence: wei_wei@whut.edu.cn; Tel.: +86-027-86551180

Abstract: The heat exchanger plays a key role in the S-CO₂ power cycle of power generation systems based on waste heat and has a large impact on their cost control and compactness. In this paper, we take the channel shape of a microchannel heat exchanger as the research object and combine orthogonal tests and numerical simulation, taking the microchannel cross-section length/short-axis ratio, volume ratio and filling rate as independent variables, to numerically study multi-channel thermal–fluid–solid coupling and explore the effects of different microchannel cross-section length/short-axis ratios, volume ratios and filling rates on the thermal hydraulic and mechanical properties of the heat exchanger. The results show that a change in the channel volume ratio has a greater impact on the thermal hydraulic performance of the heat exchanger and that its heat transfer performance is only marginally affected by a change in the channel filling rate. Additionally, when other geometric parameters are kept to a certain level, the closer the shape of the channel is to a circle, the better its mechanical properties are. Within the range of permissible designs, a change in the channel volume ratio does not have an obvious impact on the mechanical properties of the microchannels, while the channel filling rate has the most significant impact. The most significant effect of the channel filling rate on the mechanical properties occurs through the channel volume ratio.

Keywords: microchannel heat exchanger; channel shape; heat transfer performance; mechanical properties



Citation: Li, P.; Fu, W.; Zhang, K.; Li, Q.; Zhang, Y.; Li, Y.; Wang, Z.; Hou, X.; Sun, Y.; Wei, W. Effect of Channel Shape on Heat Transfer and Mechanical Properties of Supercritical CO₂ Microchannel Heat Exchanger. *Energies* **2024**, *17*, 3774. <https://doi.org/10.3390/en17153774>

Academic Editors: Tadeusz Bohdal and Marcin Kruzel

Received: 3 June 2024
Revised: 23 July 2024
Accepted: 27 July 2024
Published: 31 July 2024



Copyright: © 2024 by the authors. Licensee MDPI, Basel, Switzerland. This article is an open access article distributed under the terms and conditions of the Creative Commons Attribution (CC BY) license (<https://creativecommons.org/licenses/by/4.0/>).

1. Introduction

Utilizing waste heat from the main engine fluid gas to build the S-CO₂ power cycle of power generation systems is an important way to save energy and reduce emissions on ships [1]. The heat transfer performance and pressure drop of heat exchanger equipment such as the heat reclaiming and pre-cooler are the key factors affecting the efficiency of these systems, and the development of printed circuit heat exchangers (PCHEs) provides strong support for the research and application of the S-CO₂ power cycle. Under the same thermal power conditions, the compactness of a PCHE is more than 85% higher than that of a traditional shell-and-tube heat exchanger, making it the ideal choice to replace these traditional exchangers [2–4]. Optimization studies of the structure of microchannel heat exchangers are of great significance in improving their heat transfer and reducing their operating costs [5,6]. Although scholars have proposed heat transfer correlation formulas for different structural forms of PCHEs, in practice, whether these formulas detail the impact of microchannel shape via the exchanger’s processing or service process will result in differences that will cause deviations between its actual and theoretical heat transfer performance. Therefore, it is necessary to consider how changing the shape of the microchannel impacts the performance of the heat exchanger to make corrections to its

design as well as provide a theoretical basis for the use of these processes in the prediction of the performance of heat exchangers.

With the continuous development of S-CO₂ power cycle research, the most common PCHE channel type for the straight channel, Z channel and wing channel has become a semicircular cross-section, while scholars have carried out a large number of studies on different channel types to investigate their effect on thermal hydraulic performance [7]. The research on PCHE flow channels started with the straight channel; Seo [8] tested the thermal hydraulic performance of water in a straight-channel PCHE and found that the average heat transfer rate and heat transfer performance of the counterflow structure were 6.8% and 10~15% higher than that of the parallel-flow structure, respectively. Keeping the inlet temperature of the cold side constant and simultaneously elevating the inlet temperature of the hot side had no effect on the PCHE heat transfer performance but could reduce pressure loss. In order to improve the heat transfer performance of PCHEs, many scholars have complicated the structure of the straight flow channel; of these complications, Z-shaped flow channels are the most widely researched and applied and, due to their high durability and manufacturability, they are the most frequently used channel in traditional-type PCHEs; however, Z-shaped channels have high pressure loss due to flow separation and backflow at their bending points. In order to improve the performance of PCHEs with Z-shaped channels, Kim [9] numerically analyzed the traditional Z-shaped channel PCHE model and designed a new PCHE using streamlined wing fins to optimize its thermal hydraulic performance; the simulation results showed that the total heat transfer rate per unit volume in the proposed PCHE was almost the same as that of sawtooth-channel PCHEs, reducing the pressure drop to one-twentieth of that of Z-shaped channel PCHEs. Zhan [10] showed that the counterflow in Z-channel PCHEs enhances their field synergy and reduces the generation of heat transfer entropy, while the secondary flow enhances the synergy of the velocity gradient and temperature gradient in the sawtooth channel and enlarges the entropy near the wall, with a bending angle between 110° and 130° exhibiting the best overall performance with respect to both the first and second laws of thermodynamics.

Yoon [11] pointed out that the shape and dimensions of individual channels of PCHEs after diffusion joining are not uniform and that the overall geometry of PCHEs may be deformed during their operation in high-temperature conditions, which may lead to inaccurate results in thermal hydraulic performance analyses based on their design parameters. Due to their configuration and the horizontal or vertical orientation of the whole heat transfer system, PCHEs are subject to thermal and mechanical deformation. Deformation of their channels will affect their operation, and in serious cases of fracture this may even lead to accidents. Therefore, it is necessary to study the thermal stress of PCHEs during their operation [12]. There are few studies on the thermal stress characteristics of PCHEs in the literature. Lee [13] investigated the structural integrity of an intermediate printed circuit heat exchanger (PCHE) in a sodium-cooled S-CO₂ fast reactor. The stress field in the flat channel of the PCHE was simulated using ANSYS-Mechanical, and the temperature field was imported from a FLUENT simulation. The mechanical stresses induced by pressure loads were found to be the main source of these stresses, which may affect the actual life of PCHEs through corrosion and fatigue. Jiang [14] performed a coupled thermal–fluid–solid analysis of PCHEs by establishing a three-dimensional thermal–fluid–solid coupling numerical model to investigate the thermal–fluid–solid coupling characteristics of PCHEs with different airfoil tail arrangements, while also studying the stress distribution of a single airfoil fin to obtain a better airfoil arrangement that accounted for the system’s heat transfer characteristics and stress distribution. Wang [15] used a finite element method to evaluate the structural strength of a hybrid microchannel heat exchanger, and their results showed that the thermal stress caused by the temperature gradient was independent of the absolute temperature values. Furthermore, the change in S-CO₂ pressure in the etching channel had a bigger effect on the exchanger’s mechanical stresses than the spent gas pressure in the fin channel did, while thermal and mechanical stresses contributed equally to the total stresses on the hybrid heat exchanger under the designed conditions.

The heat exchanger plays a key role in the S-CO₂ power cycle of power generation systems based on waste heat and has a large impact on its cost control and compactness; therefore, it is extremely important to optimize the design of the heat exchanger to improve the performance of the entire system. Most researchers have focused on the shape of the flow channel in the direction of the flow line, such as straight channels, Z-channels, etc., while fewer have focused on the effect of the flow channel's cross-section on the heat transfer and mechanical properties of microchannel heat exchangers. This paper takes the flow channel's cross-section as its research object and carries out a multi-channel thermal–fluid–solid coupling numerical simulation to investigate the influence of its structural parameters on the heat transfer performance and mechanical properties of a heat exchanger. Starting from the actual conditions experienced during the operation of a PCHE, it provides a theoretical basis for the design of heat exchangers as well as the prediction of their heat transfer performance during use.

2. Thermal–Fluid–Solid Coupling Analysis Methods

During its operation, a microchannel heat exchanger experiences decreasing pressure and temperature, i.e., its channels are subjected to uneven pressure and temperature loads. In the design process, these are generally theoretically assumed to be a uniform pressure and temperature, with designs for maximum pressure, maximum temperature or average temperature made accordingly, resulting in a relatively large redundancy, unnecessary waste and other serious consequences. In order to avoid similar situations, a more realistic reflection of the microchannel heat exchanger's thermal hydraulic performance and stress distribution is required; thus, this paper uses the thermal–fluid–solid coupling method to optimize the design of microchannel heat exchangers.

Thermal–fluid–solid coupling, as the name suggests, is the coupling between the temperature field, flow field and solid deformation. The general process of thermal–fluid–solid coupling is to use the results obtained from a flow field analysis as the load and the coupling interface as the carrier; the role of this analytical research is to provide information to create an accurate numerical model that simulates the actual working state of the heat exchanger. Through this numerical calculation method, the temperature field, stress field and other parameters of the heat exchanger can be found.

In order to assess the thermal hydraulic characteristics of the microchannel heat exchanger, it is necessary to quantitatively analyze specific related parameters; in this paper, we chose to examine the surface convective heat transfer coefficient h , Nusselt number Nu , etc.

As the channel structures in this paper are semicircular, their hydraulic diameter is introduced through the calculation of the Reynolds number, which is calculated by the following formula:

$$D_h = \frac{4A}{C} \quad (1)$$

where A denotes the cross-sectional area of the channel in mm² and C is the cross-sectional perimeter in mm.

The equations in this paper, including the fitting correlation equation, involve the Reynolds number and Prandtl number. The Reynolds number Re is calculated as follows:

$$Re = \frac{\rho v D_h}{\mu} \quad (2)$$

where μ is the coefficient of dynamic viscosity in Pa-s.

The Prandtl number Pr is calculated as follows:

$$Pr = \frac{C_p \mu}{\lambda} \quad (3)$$

where C_p denotes the constant-pressure-specific heat capacity of S-CO₂ at the reference temperature and λ is the thermal conductivity of S-CO₂ at the reference temperature.

In this paper, the average convective heat transfer coefficient is chosen to represent the heat transfer characteristics of S-CO₂ in the microchannel, and this is calculated as follows:

$$h = \frac{q}{T_b - T_w} \quad (4)$$

where q denotes the heat flow density in W/m²; T_w denotes the average temperature of the thermal channel's wall in K; T_b denotes the average temperature of the S-CO₂ in the mainstream region of the thermal channel in K.

The pressure drop can be obtained directly via numerical simulation.

In order to quantitatively evaluate the flow and heat transfer characteristics of S-CO₂ in the microchannel, this paper introduces the Nusselt number Nu , Colburn factor j , friction factor f , G_v , etc. j is the index for evaluating the performance of the heat exchanger and its degree of compactness; a larger j indicates a better performance and degree of compactness. G_v is the comprehensive evaluation of the flow and heat transfer in the heat exchanger and, similarly, the larger the G_v , the better the flow and heat exchange in the heat exchanger. These are defined as follows:

$$Nu = \frac{hD_h}{\lambda} \quad (5)$$

$$j = \frac{Nu}{RePr^{1/3}} \quad (6)$$

$$f = \frac{\Delta PD_h}{2\rho\bar{v}^2L} \quad (7)$$

$$G_v = \frac{j}{f^{1/3}} \quad (8)$$

3. Numerical Modeling and Validation

Figure 1a displays the numerical simulation of a PCHE as a geometric model and the schematic of its cross-section parameters. Countercurrent hot and cold fluids enable heat transfer; in order to exclude the import and export effects of the hot and cold channels, the hot and cold fluid inlet and outlet sections are extended to the fluid domain. To facilitate the full development of the inlet flow and to stabilize the outlet flow, the length of each fluid field, excluding extensions, is 300 mm. The fluid and solid parts of the model are meshed in hexahedrons, separately and combined together, with a minimal orthogonal quality value of 0.7, as shown in Figure 1b.

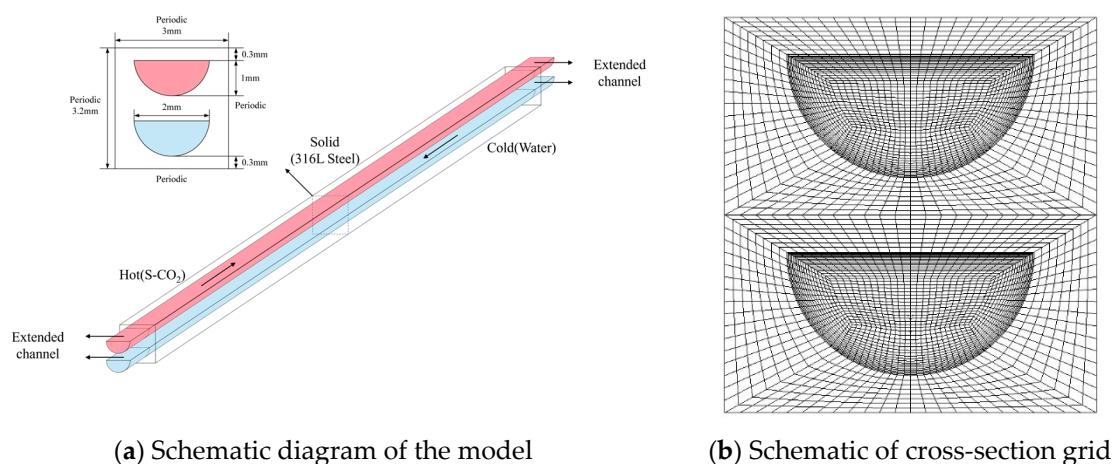


Figure 1. Schematic of model and cross-section grid.

Due to the large temperature dependence of the physical properties of S-CO₂, its main physical properties, such as its density, specific heat capacity, thermal conductivity, kinetic viscosity, and others, were extracted by interpolation through the NIST REFPROP database using the system's operating pressure and temperature range as shown in Figure 2, and numerical simulations were performed using user-defined materials from FLUENT 2020 r2, with the boundary conditions set as follows:

- (1) The inlet of the cold and hot channels were set as mass flow inlets and their outlets as pressure outlets;
- (2) The cold and hot fluid and solid interfaces were established as coupled interfaces for heat exchange;
- (3) The solid domain is set up with periodic boundary conditions around it, as shown in the cross-section of Figure 1a.

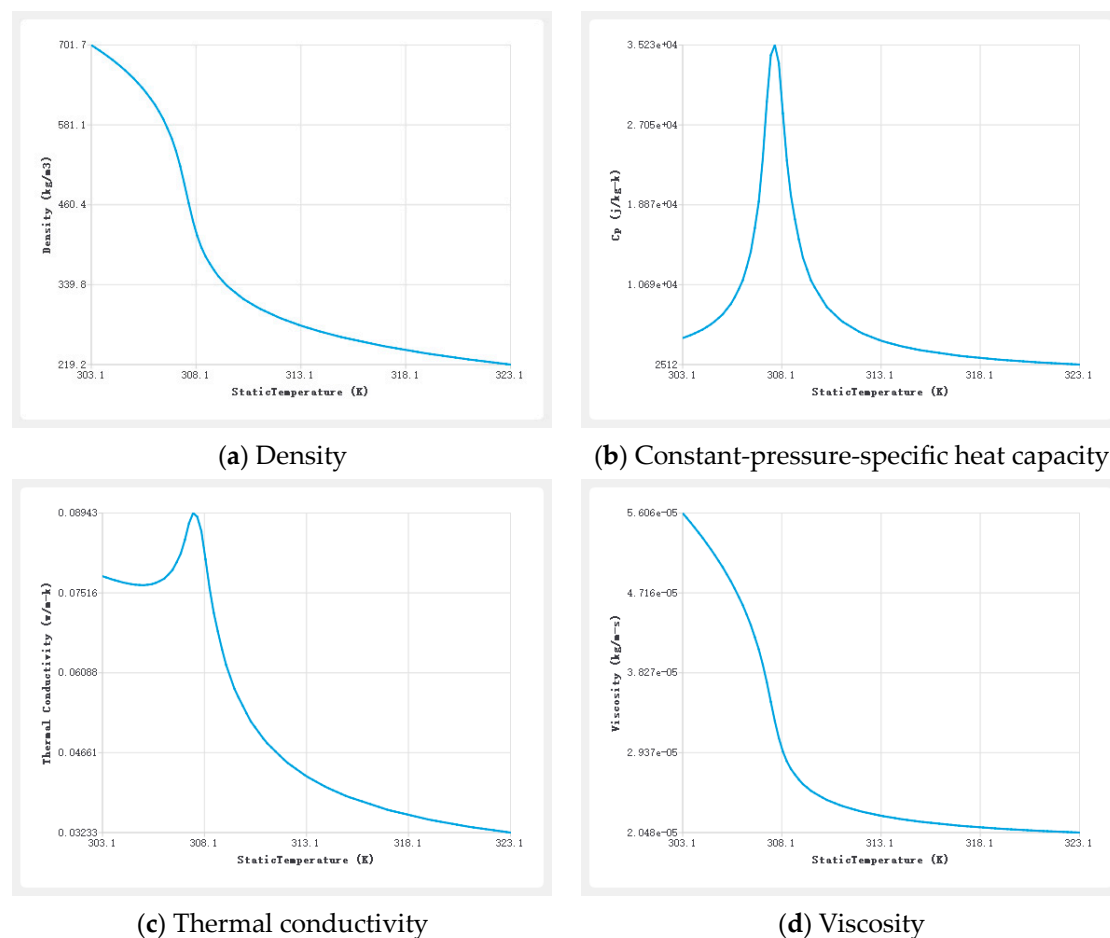


Figure 2. Physical properties variation of S-CO₂ (8.0 MPa).

The S-CO₂ water heat transfer test was conducted using the test platform and is shown in Figure 3. During the experiment, CO₂ flowed out of the CO₂ tank, which was pressurized by a gas booster to above its critical pressure and regulated by a buffer tank. Next, CO₂ entered the heater for and then entered the PCHE as the hot fluid for heat transfer. The pressure, pressure difference and temperature of the CO₂ were measured at the inlet and outlet of the PCHE. Then, the CO₂ that had completed the heat exchange process flowed through the cooler connected to the chiller to cool down and then circulated to the gas booster. The water on the other side was provided by a chiller. The operating pressure on the water side was atmospheric pressure. During the test, after the flow rate, inlet/outlet pressure, inlet/outlet pressure difference and inlet/outlet temperature parameters reached stable states, the next set of working conditions was considered.

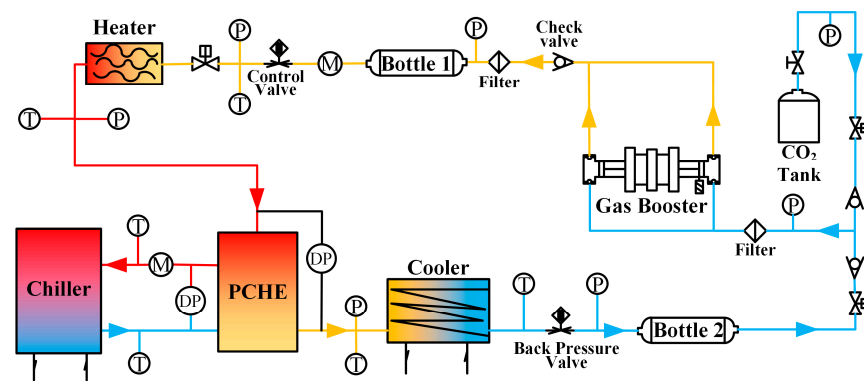


Figure 3. System schematic of the PCHE test [7].

The numerical simulation method used in this paper has been validated by our team's previous work as being accurate and effective [7]. Five groups of experimental data spanning the inlet Reynolds number, from 4500 to 15,500, were selected as the control, as shown in Table 1, and the numerical simulation was carried out under the test conditions. S-CO₂ outlet temperature comparison between the obtained numerical simulation results and the experimental results is shown in Figure 4, which demonstrates that the thermodynamic temperatures of the outlet obtained using both methods match well under different operating pressures, inlet temperatures and inlet flow rates.

Table 1. Experimental working conditions.

Serial Number	1	2	3	4	5
Operating pressure/MPa	9.5	9.0	8.8	8.95	8.78
Hot-side inlet temperature/K	328.7	312.02	318.7	313.72	312.85
Cold-side inlet temperature/K	289.15	298.15	297.15	298.15	297.15
Hot-side Reynolds number	15,428	4734	9980	7848	8963
Hot-side flow rate/g·s ⁻¹	0.4635	0.238	0.3073	0.3214	0.3611
Cold-side flow rate/g·s ⁻¹	0.2282	0.2352	0.5763	0.2359	0.6053

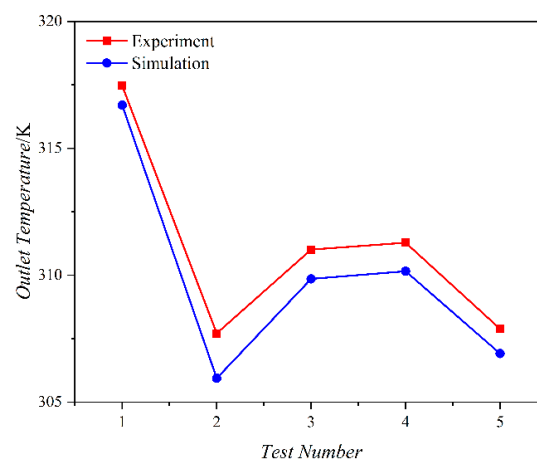


Figure 4. Outlet temperature verification.

After verifying the above five groups of test conditions through numerical simulation, it was found that the temperature difference between the S-CO₂ inlet and outlet was large under condition 3, crossing the proposed critical zone under the corresponding pressure. The temperature range at this condition spans the pseudo-critical point of S-CO₂. Condition 3 was thus chosen for the numerical simulation in order to compare the differences in the thermal hydraulic performance of different channel shapes under drastic changes in the physical properties of S-CO₂, as shown in Figure 5.

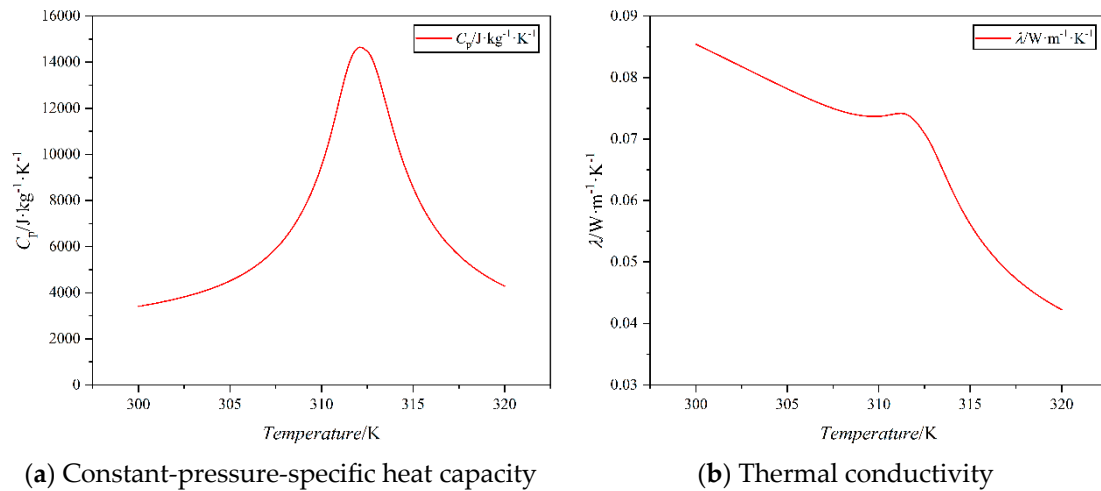


Figure 5. Changes in S-CO₂ physical properties in the operating range of condition 3.

4. Influence of Channel Cross-Section on Thermal Hydraulic Performance

As shown in Figure 6, important dimensional parameters of the channel (channel width a , channel height b , wall width L and wall height H) are used to define its shape in terms of the ratio of the length/short axis of its cross-sectional shape a/b , to define its channel volume ratio (which characterizes the size of the interchannel spacing relative to the size of the PCHE plate sheet) in terms of the ratio of the area of the inner semicircular channel to the area of the outer rectangle, and to define its channel filling ratio (which characterizes the size of the interchannel space between the transverse space and longitudinal space), so that we can explore the change in the overall performance of the microchannel heat exchanger in light different shapes and structural parameters.

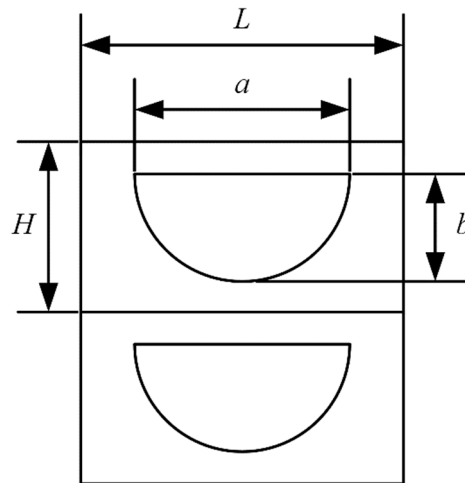


Figure 6. Schematic diagram of the channel's shape and parameters.

When S-CO₂ exchanges heat with water in the cold channel, its physical properties in the hot channel of the PCHE change with the decrease in temperature and pressure, especially when crossing the proposed critical zone, where its physical properties change more drastically. By segmenting the numerical model of the PCHE along the direction of its flow, the cross-section of the fluid domain is intercepted from the middle of the model to the two ends of the perimeter line segments of the cross-section at intervals of 0.02 m; this cross-section is used to extract the average physical quantity of the fluid in that place as the local fluid value, and the perimeter line segment is used to extract the average physical quantity of the wall in that place as the local wall value. The cross-section of the fluid domain

is used as a symmetry plane, and 0.001 m of the wall at each end of the channel is used to extract the average heat flow density as the local value of the heat flow density in that area.

4.1. Influence of Channel Cross-Section on Thermal Hydraulic Performance

With a fixed volume ratio and fill rate constant ($\frac{a/b}{L/H} = 1$, $\frac{ab}{LH} = \frac{5}{12}$), and while keeping the cross-sectional area of the channel constant, the a/b ratio can be changed to change the cross-sectional shape of the channel. The changes in the long-range local surface heat transfer coefficient and Nu number along the flow direction in hot runners with different cross-sectional shapes are shown in Figure 7. Both show the same trend of first increasing and then decreasing as the flow of S-CO₂ inside the channel increases, which is related to the change in the physical properties of the long-range S-CO₂ inside the channel. This is related to the physical change in the S-CO₂ within the channel, with the heat transfer and temperature of the S-CO₂ and the channel wall decreasing. However, the C_p of S-CO₂, as the temperature changes, shows a trend of first increasing and then decreasing. When the C_p is larger during the release of the S-CO₂, the temperature decreases by less, resulting in the existence of a minimum in the temperature difference between the S-CO₂ and the wall surface, which corresponds to the maximum coefficient of heat transfer for the local surface, while, with the decrease in temperature, the thermal conductivity of S-CO₂ rises, leading to Nu also showing a trend of first rising and then falling.

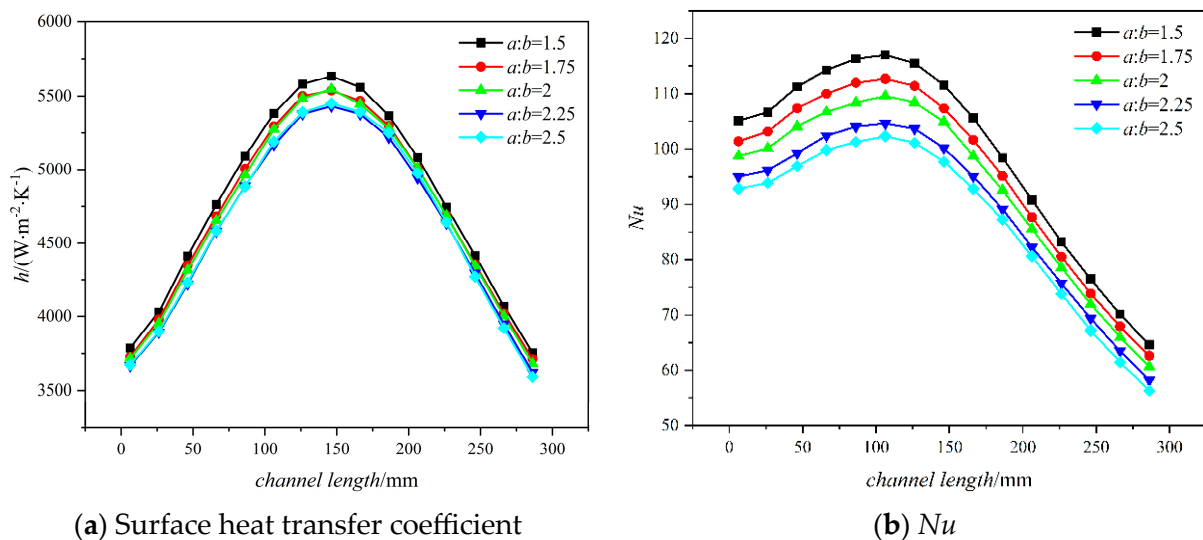


Figure 7. Distribution of h and Nu with different a/b ratios.

From the variation in the local surface's heat transfer coefficient versus Nu , it can be seen that a reduction in the a/b ratio non-significantly improves the heat transfer performance of the channel when the channel area remains the same. However, according to the variation in total heat transfer with respect to the total pressure drop, as shown in Figure 8, while a larger a/b ratio can obtain greater heat transfer, it leads to a larger pressure drop, which is due to the fact that a channel with a larger a/b ratio has a larger heat transfer area and can conduct more heat transfer with little change in its heat transfer performance. However, it consequently also loses relatively more pressure.

A comparison of the heat exchanger's j factor and G_v for channels with different a/b ratios is shown in Figure 9; with the increase in a/b ratio, both the j factor and G_v decrease. Although the heat exchanger can conduct more heat exchange under a larger a/b ratio, with a comprehensive consideration of the flow and heat exchange, channels with a smaller a/b ratio shape have better thermal hydraulic performance.

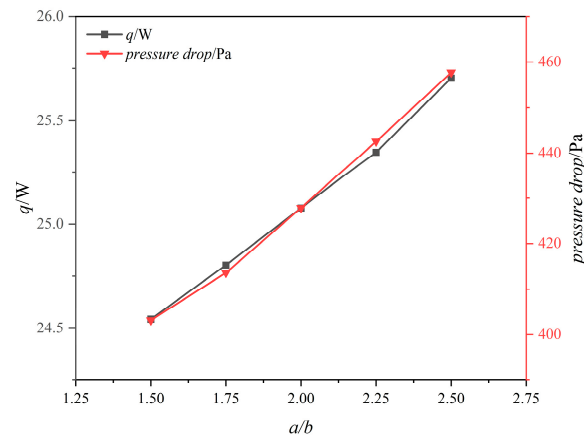


Figure 8. Variation of total heat transfer and total pressure drop with different a/b ratios.

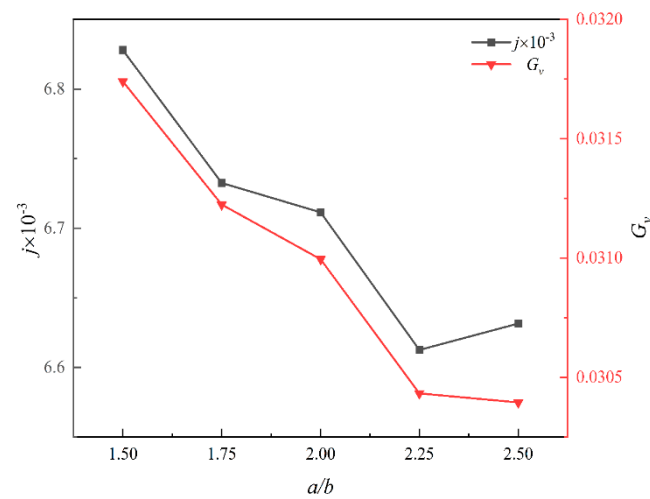


Figure 9. The j factor vs. G_v at different a/b ratios.

4.2. Effect of Channel Volume Ratio on Thermal Hydraulic Performance

While maintaining the same operating conditions, we let $a/b = 2$ (meaning that the cross-sectional shape of the channel was semicircular), $\frac{a/L}{b/H} = 1$. Given the cross-sectional shape and filling ratio, the values of $b = 0.5a$ taken into consideration were 0.8 mm, 0.9 mm, 1.0 mm, 1.1 mm and 1.2 mm, which were used to investigate how different cross-sectional areas change the thermal hydraulic performance of these channels. The local surface heat transfer coefficients along the length of thermal channels with different cross-sectional areas are shown in comparison to their Nu in Figure 10. Through this comparison, it becomes apparent that with the reduction in the semicircular cross-section radius of the channel, the local surface heat transfer coefficients along the channel increased significantly, which is due to the inlet mass flow rate being kept constant. Reducing the channel's cross-sectional area increases the channel's fluid flow rate and Re significantly, thus improving the local heat transfer effect along the length of the thermal channel; further, with the reduction in the radius, the local surface heat transfer coefficients along the length of the thermal channel, in terms of Nu , increase dramatically. The local surface heat transfer coefficients are also much larger, and the location of their maximum value within the channel has a tendency to move slightly toward the entrance, which is because the fluid temperature in the hot channel decreases and reaches the point of its maximum C_p value faster due to the enhancement of local heat transfer, which means that the local surface heat transfer coefficient in the channel reaches its maximum value earlier. At the same time, it can be observed that when the radius of the semicircular cross-section of the channel is small, the local surface heat transfer coefficient of the outlet section is smaller than that of the inlet

section and, with the increase in the radius, the local surface heat transfer coefficient of the outlet section increases relative to that of the inlet section, which is also associated with the change in the physical properties of the S-CO₂. This leads to the local surface heat transfer coefficient of the outlet section being larger than that of the inlet section.

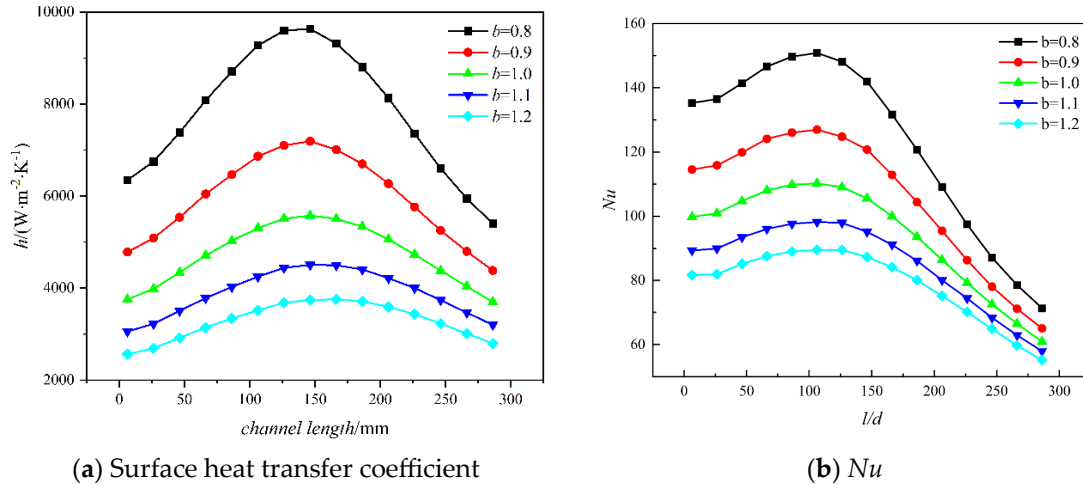


Figure 10. Distribution of h and Nu with different cross-sectional areas.

Compared to the channel’s cross-sectional shape, the change in its cross-sectional area has a greater impact on its thermal hydraulic performance, as shown in Figure 11, which compares the total heat transfer coefficients of heat exchangers with different channel cross-sectional areas. With the increase in channel radius, i.e., an increase in cross-sectional area, the total heat transfer coefficient of the heat exchanger decreases significantly, which is due to the fact that, under the same working conditions (the same mass flow rate), channels with smaller cross-sectional areas have a larger flow rate and Re , which effectively enhances the convective heat transfer of their work fluid. Similarly, the variations in the j factor and G_v under different cross-sectional areas show the same trend, as shown in Figure 12; channels with smaller cross-sectional areas have a larger j factor and G_v , which indicates that, under the same working conditions, reducing the cross-sectional area of the channel (or increasing the flow rate of the mass in the channel) allows the heat exchanger to obtain a better heat transfer performance.

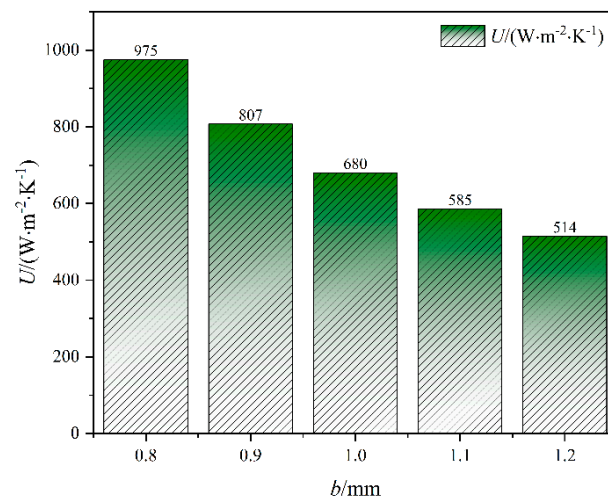


Figure 11. Comparison of total heat transfer coefficients of heat exchangers with different channel cross-sectional areas.

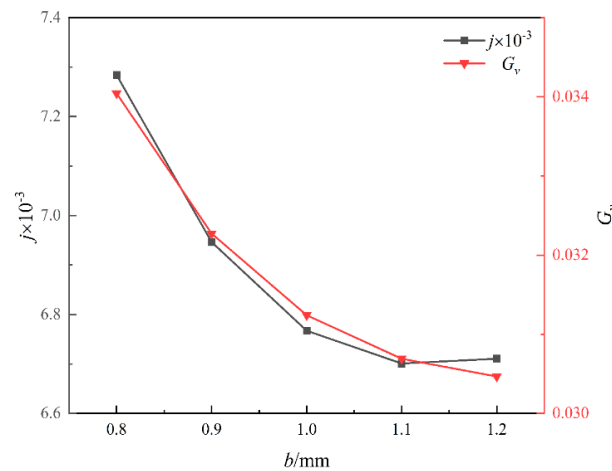


Figure 12. The j factor vs. G_v for heat exchangers with different channel cross-sectional areas.

4.3. Effect of Channel Fill Rate on Thermal Hydraulic Performance

Since the PCHE heat exchanger is formed by a cyclic combination of multiple hot and cold channels, the top, bottom, left and right walls of the model are set as cyclic boundary conditions, within which the shape and size of the channels do not change: $\frac{a/L}{b/H}$. The change in the $\frac{a/L}{b/H}$ ratio represents the change in the transverse and longitudinal spacing of adjacent channels. When it is equal to a/b , this indicates that the transverse and longitudinal spacing of adjacent channels are the same as the size of the channel flowing in the same direction. An increase in the $\frac{a/L}{b/H}$ ratio indicates that the longitudinal spacing of adjacent channels decreases and their transverse spacing increases, and, vice versa, a reduction indicates that the longitudinal spacing of adjacent channels increases and their transverse spacing decreases.

When keeping $\frac{a/L}{b/H}$, a/b , and the channel’s shape and volume ratio unchanged, the filling ratio of the channel is changed by changing its solid domain aspect ratio, L/H . As shown in Figure 13, the local surface heat transfer coefficient and Nu of a channel change along its length and with different values of $\frac{a/L}{b/H}$. Since the shape and size of the heat transfer channel are unchanged, the change in heat transfer performance brought about by the change in the L/H ratio is not large; however, in general, a smaller L/H ratio leads to a better heat transfer effect.

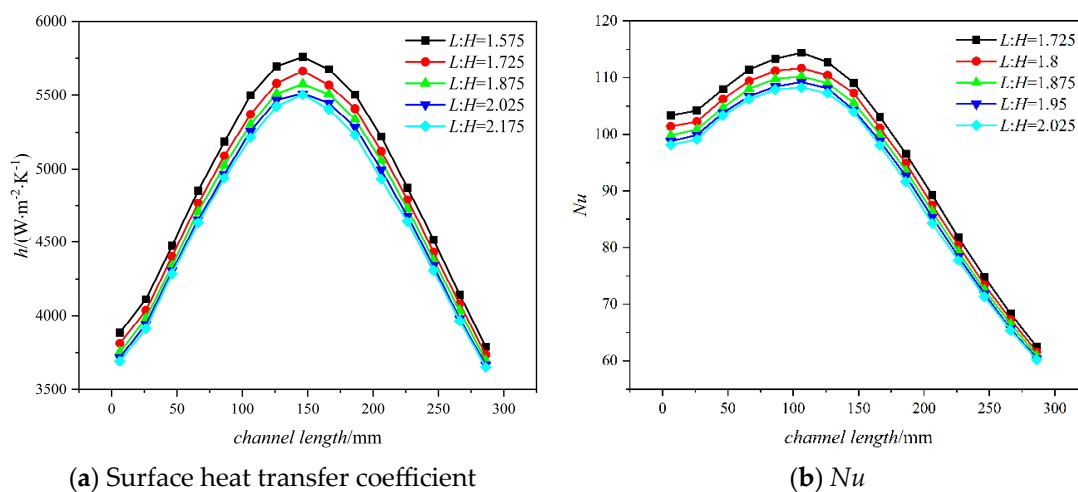


Figure 13. Distribution of h and Nu with different channel lengths.

5. Effect of the Channel’s Cross-Section on Its Mechanical Properties

In this section, we analyze the mechanical properties of different channel shapes by ANSYS-Mechanical 2020 r2. The type of stress analysis used in this paper is an equivalent

stress analysis; because the forces used in actual engineering analyses are complex and variable, it is difficult to determine the axial tensile and compressive condition at a single point. As such, it is more convenient to use an equivalent stress analysis. Von Mises stress is a kind of equivalent stress which simulates the distribution of stresses inside an object through stress contours. The stress distribution inside an object can clearly reflect the change in stress within it, and thus quickly determines the part of the model subjected to the highest stress.

The stress–strain distribution of $a/b = 2$, $b = 0.8$ mm and $\frac{a/L}{b/H} = 1$ under an operating pressure of 8.8 MPa and an inlet Reynolds number of 5000 on the hot side is shown in Figures 14–16. The stress–strain distribution of the microchannel decreases in the direction of the S-CO₂ flow, which is mainly due to the fact that its temperature decreases in this direction, and its thermal stress is also decreased, while the mechanical stresses caused by the pressure drop have relatively little effect. The main reason for this is that there is a gradual decrease in thermal stresses in this direction. The maximum stress and strain are both on the hot side's inlet wall, and the maximum stress is concentrated below the arc of the cold-side channel.

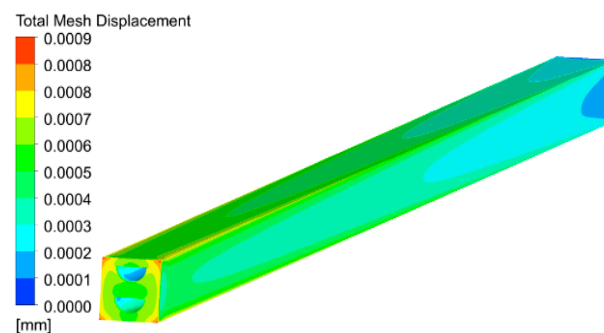


Figure 14. Microchannel deformation distribution cloud.

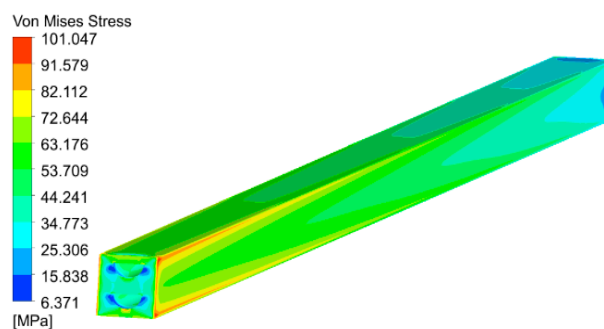


Figure 15. Cloud diagram of distribution of Von Mises equivalent stress in microchannel.

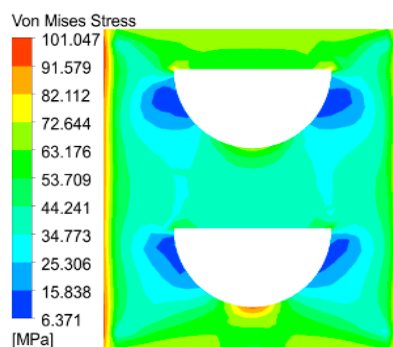


Figure 16. Cloud view of Von Mises equivalent stress distribution on the thermal inlet side of the microchannel.

5.1. Effect of Channel Cross-Section on Mechanical Properties

We extracted the stress–strain distribution of the PCHE hot and cold dual-channel arc segments and straight line segments, as shown in Figure 17. At $a/b = 1.5$, as shown in Figure 18, the maximum stress is concentrated in the middle-most position of the cold-side channel's arc segments and is symmetrically distributed along their center, while the maximum strain occurs at the point where the arched side of the hot channel's cross-section meets its straight side, which is a relatively small point compared to the radius of the microchannels.

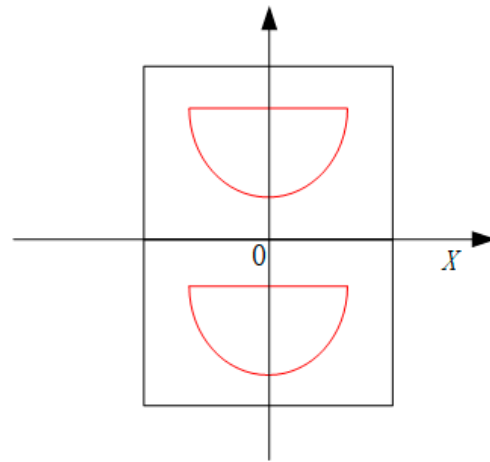


Figure 17. Extraction path and axes.

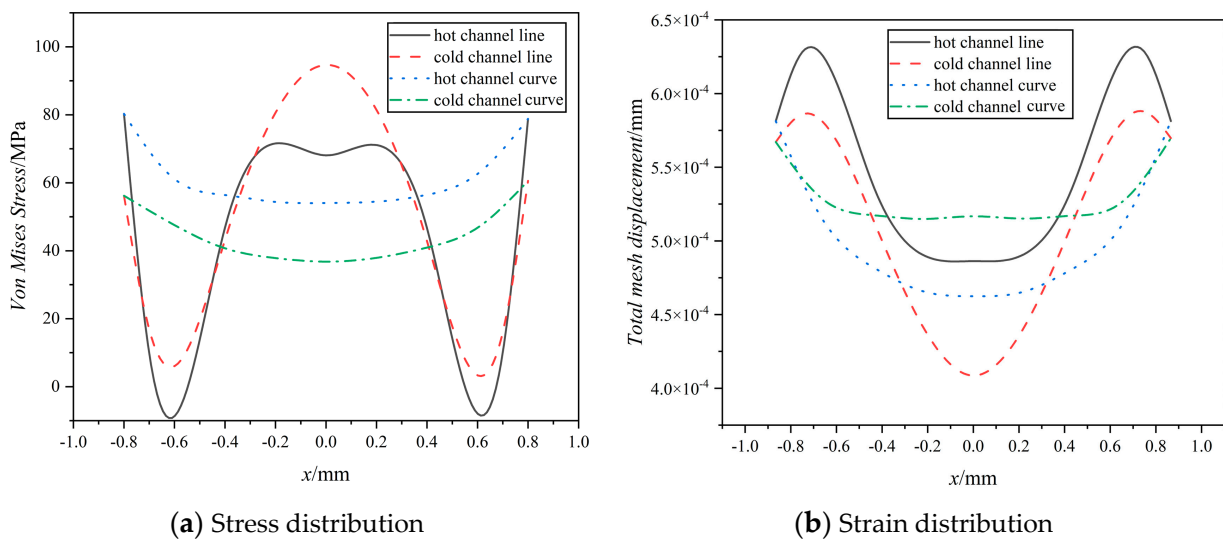


Figure 18. Stress–strain distribution at different positions.

Different a/b ratios mainly affected the numerical value of the stress–strain distribution, as the distribution trend did not change significantly. For further analysis, we selected the maximum stress and minimum stress in the channel in order for the range of stress to be analyzed; Figure 19 shows the maximum stress distribution and stress range at different a/b ratios. With the increase in a/b , the maximum stress and stress range also increased. At $a/b = 2.5$, compared to $a/b = 1.5$, the maximum stress increased by about 15% and the stress range increased by about 54%; it can be concluded that a smaller a/b ratio leads to good mechanical properties when other geometrical parameters are kept constant.

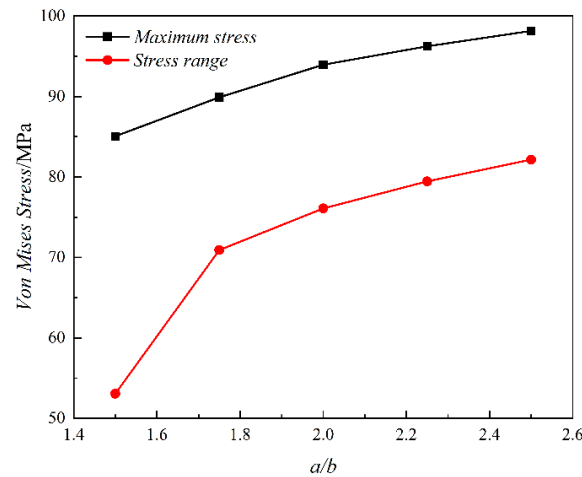


Figure 19. Maximum stress and range of stress at different a/b ratios.

5.2. Effect of Channel Volume Ratio on Mechanical Properties

Taking the channel radius $b = 0.8$ mm as an example, we can see that the stress–strain distribution of different cross-section shapes is similar, as shown in Figure 20. Here, the stress and strain are symmetrically distributed along the center; the strain is the largest near the connection between the straight section and the arc section of the channel, but relatively small overall, while the stress basically remains the largest in the middle of the cold-side channel.

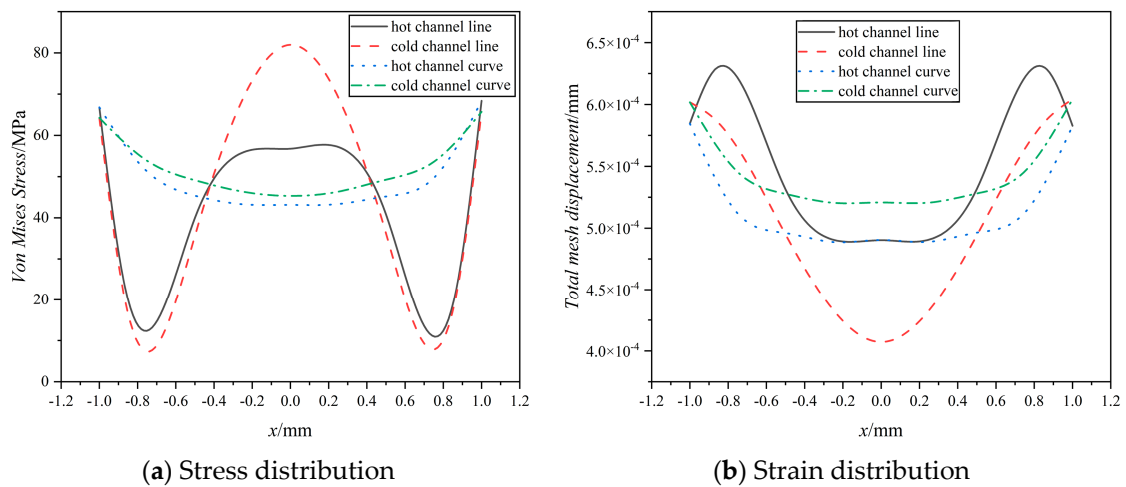


Figure 20. Stress–strain distribution at different positions along the channel.

Similarly, to further analyze the effect of different channel radii on the distribution of stress and strain, the maximum stress and the stress range in the microchannel will be selected for analysis. As shown in Figure 21, if the other geometric parameters of the channel remain unchanged, as the radius increases, the maximum stress increases. This is mainly due to the increase in the channel radius leading to the spacing and thickness of the channel wall decreasing; using the same material, under the same service conditions, the thickness required to withstand a smaller stress is larger. The maximum stress on the channel with a radius $b = 1.2$ mm increases by only 12% compared to the channel with the radius $b = 0.8$ mm. The effect of the channel radius on the stress range is even smaller, increasing by only 8% and decreasing at a channel radius $b = 1$ mm. It is concluded that the change in channel radius does not have a significant effect on the mechanical properties of microchannels within the allowable design range.

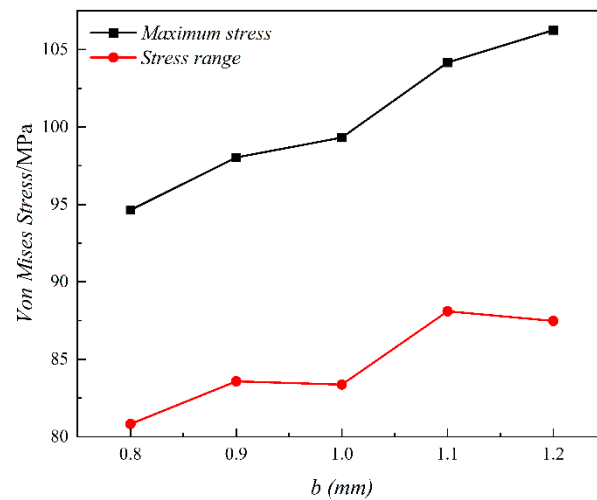


Figure 21. Distribution of maximum stress and stress range for different bs.

5.3. Effect of Channel Filling Ratio on Mechanical Properties

Taking the aspect ratio $L/H = 1.575$ as an example, the stress–strain distribution of the arc and straight line segments of the cold and hot channels is extracted as shown in Figure 22. These are similar to those of microchannels with different cross-sectional shapes and different channel radii, as above; the stress distribution is at its maximum in the middle of the arc segment of the cold-side channel and distributed symmetrically along the center, while the strain distribution is similarly at its maximum in the vicinity of the connection between the arc segment and the straight line segment in the hot-side channel.

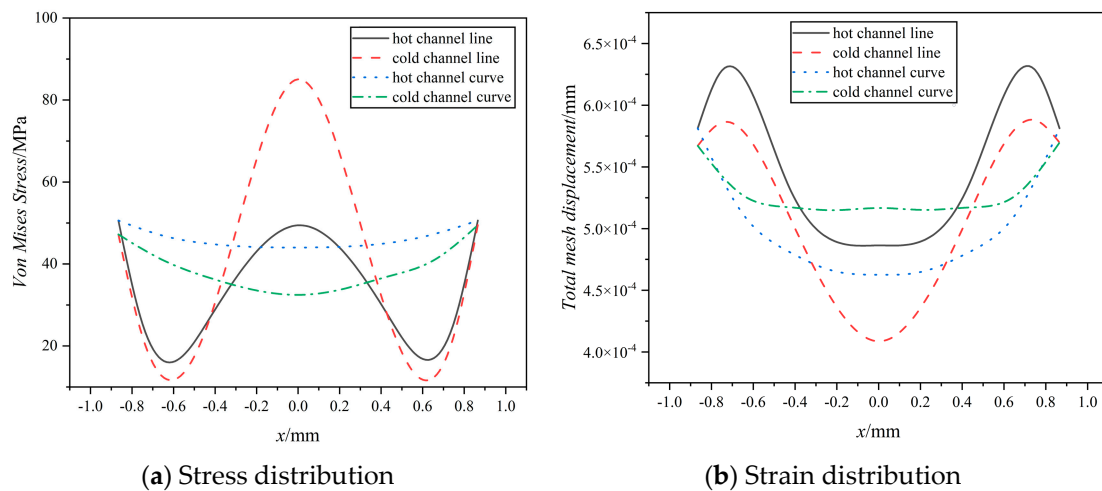


Figure 22. Stress–strain distribution at different lengths along the channel.

Similarly, to further analyze the effect of different channel spacings on the stress–strain distribution within the channel, the maximum stress and the range of stress in a selected microchannel will be analyzed. As shown in Figure 23, when other geometric parameters of the microchannel remain unchanged, an increase in L/H leads to an increase in the maximum stress and the range of stress. That is, the smaller the channel spacing, the greater the stress endured. When $L/H = 2.175$, the maximum stress increases by 42% compared to that at $L/H = 1.575$, and the maximum stress range increases by 67%.

In summary, a single-variable control method was adopted to analyze the effects of the cross-sectional shape, volume ratio and filling rate of microchannels on the PCHE mechanical properties. It can be concluded that, under the condition that the other geometric parameters remain unchanged, the microchannel’s filling rate has the most significant

effect on its mechanical properties, while, within the permissible design range, the channel volume ratio has the weakest effect.

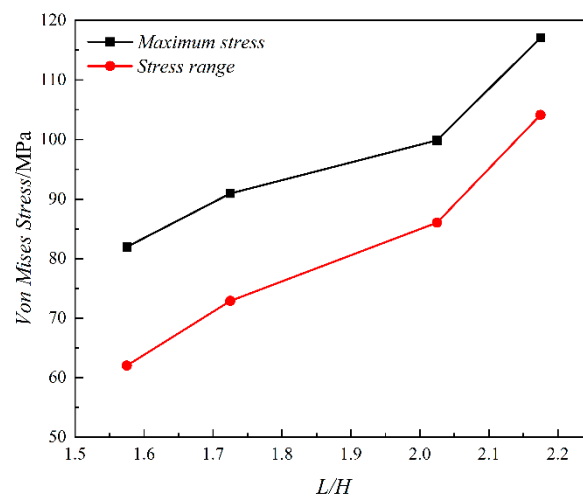


Figure 23. Maximum stress and stress range at different L/H ratios.

6. Conclusions

This paper utilizes the thermal–fluid–solid coupling method to simulate a microchannel heat exchanger with different channel shapes and structures and discusses the effects of different microchannel cross-sections, long/short axis ratios, volume ratios and filling rates on the hydraulic and mechanical properties of the heat exchanger. Our main conclusions are as follows:

(1) Combined with orthogonal tests and numerical simulations, multi-channel thermal–fluid–solid coupling studies were carried out on the microchannel’s cross-section, utilizing the long/short axis ratio, volume ratio and filling rate as the optimization parameters. The effects of these individual structural parameters on the heat exchanger’s performance and flow resistance were analyzed using the variable control method.

(2) When ensuring the other variables are unchanged, the channel volume ratio has a greater impact on the PCHE thermal hydraulic performance than the channel’s cross-sectional shape, while the change in performance caused by the channel filling ratio is relatively small.

(3) The maximum stress and the maximum strain of the system are located on the hot side’s inlet wall, with the maximum stress concentrated under the arc of the cold-side channel; when other geometrical parameters are kept constant, the smaller the a/b ratio is, the better the system’s mechanical properties are. Within the permissible design range, the channel volume ratio does not have a significant effect on the mechanical properties of the microchannel, while the channel filling rate has the most significant effect.

Author Contributions: Methodology, software, writing—original draft preparation, P.L.; validation, software, data curation, W.F.; software, validation, K.Z.; software, validation, Q.L.; methodology, formal analysis, Y.Z.; software, methodology, Y.L.; software, validation, Z.W.; methodology, writing—review and editing, X.H.; writing—review and editing, supervision, Y.S.; conceptualization, methodology, project administration, W.W. All authors have read and agreed to the published version of the manuscript.

Funding: This research received no external funding.

Data Availability Statement: Data are contained within the article.

Conflicts of Interest: The authors declare no conflict of interest.

References

1. Pan, P.; Yuan, C.; Sun, Y.; Yan, X.; Lu, M.; Bucknall, R. Thermo-economic analysis and multi-objective optimization of S-CO₂ Brayton cycle waste heat recovery system for an ocean-going 9000 TEU container ship. *Energy Convers. Manag.* **2020**, *221*, 113077. [[CrossRef](#)]
2. Fan, J.X.; Yeom, E. Numerical investigation on thermal hydraulic performance of supercritical LNG in PCHEs with straight, zigzag, and sinusoidal channels. *J. Vis.* **2022**, *25*, 247–261. [[CrossRef](#)]
3. Oh, C.H.; Kim, E.S.; Patterson, M. Design Option of Heat Exchanger for the Next Generation Nuclear Plant. *J. Eng. Gas Turbines Power-Trans. ASME* **2010**, *132*, 697–707. [[CrossRef](#)]
4. Huang, C.Y.; Cai, W.H.; Wang, Y.; Liu, Y.; Li, Q.; Li, B. Review on the characteristics of flow and heat transfer in printed circuit heat exchangers. *Appl. Therm. Eng.* **2019**, *153*, 190–205. [[CrossRef](#)]
5. Ding, M.; Liu, J.; Cheng, W.L.; Huang, W.-X.; Liu, Q.-N.; Yang, L.; Liu, S.-Y. An adaptive flow path regenerator used in supercritical carbon dioxide Brayton cycle. *Appl. Therm. Eng.* **2018**, *138*, 513–522. [[CrossRef](#)]
6. Adak, A.K.; Tewari, P.K. Technical feasibility study for coupling a desalination plant to an Advanced Heavy Water Reactor. *Desalination* **2014**, *337*, 76–82. [[CrossRef](#)]
7. Liu, B.; Lu, M.; Shui, B.; Sun, Y.; Wei, W. Thermal-hydraulic performance analysis of printed circuit heat exchanger precooler in the Brayton cycle for supercritical CO₂ waste heat recovery. *Appl. Energy* **2022**, *305*, 117923. [[CrossRef](#)]
8. Seo, J.W.; Kim, Y.H.; Kim, D.; Choi, Y.-D.; Lee, K.-J. Heat Transfer and Pressure Drop Characteristics in Straight Microchannel of Printed Circuit Heat Exchangers. *Entropy* **2015**, *17*, 3438–3457. [[CrossRef](#)]
9. Kim, M.S.; Ahn, Y.; Kim, B.; Lee, J. Study on the supercritical CO₂ power cycles for landfill gas firing gas turbine bottoming cycle. *Energy* **2016**, *111*, 893–909. [[CrossRef](#)]
10. Zhang, H.Y.; Guo, J.F.; Huai, X.L.; Cheng, K.; Cui, X. Studies on the thermal-hydraulic performance of zigzag channel with supercritical pressure CO₂. *J. Supercrit. Fluids* **2019**, *148*, 104–115. [[CrossRef](#)]
11. Yoon, S.J.; O'Brien, J.; Sabharwall, P.; Wegman, K.R.; Sun, X. Study on effects of heat loss and channel deformation on thermal-hydraulic performance of semicircular straight channel. *J. Therm. Sci. Eng. Appl.* **2018**, *10*, 041013. [[CrossRef](#)]
12. Wang, J.; Yan, X.; Lu, M.; Sun, Y.; Wang, J. Structural Assessment of Printed Circuit Heat Exchangers in Supercritical CO₂ Waste Heat Recovery Systems for Ship Applications. *J. Therm. Sci.* **2022**, *31*, 689–700. [[CrossRef](#)]
13. Lee, Y.; Lee, J.I. Structural assessment of intermediate printed circuit heat exchanger for sodium-cooled fast reactor with supercritical CO₂ cycle. *Ann. Nucl. Energy* **2014**, *73*, 84–95. [[CrossRef](#)]
14. Jiang, T.; Li, M.J.; Wang, W.Q.; Li, D.; Liu, Z. Fluid-Thermal-Mechanical Coupled Analysis and Optimized Design of Printed Circuit Heat Exchanger with Airfoil Fins of S-CO₂ Brayton Cycle. *J. Therm. Sci.* **2022**, *31*, 2264–2280. [[CrossRef](#)]
15. Wang, J.; Sun, Y.; Lu, M.; Wang, J.; Yan, X. Structural stress analysis of hybrid heat exchangers in the S-CO₂ power cycle for marine waste heat recovery. *Therm. Sci.* **2023**, *27*, 811–823. [[CrossRef](#)]

Disclaimer/Publisher's Note: The statements, opinions and data contained in all publications are solely those of the individual author(s) and contributor(s) and not of MDPI and/or the editor(s). MDPI and/or the editor(s) disclaim responsibility for any injury to people or property resulting from any ideas, methods, instructions or products referred to in the content.